

An improved linear time-varying reactive hydrodynamic control for a grid-connected wave energy conversion system

Hafiz Ahsan Said*, Demián García-Violini*^{†‡}, and John V. Ringwood*

*Centre for Ocean Energy Research (COER), Dept. of Electronic Engineering, Maynooth University, Co. Kildare, Ireland
e-mail: hafiz.said.2020@mumail.ie (corresponding author), ddgv83@gmail.com, john.ringwood@mu.ie

[†]Departamento de Ciencia y Tecnología, Universidad Nacional de Quilmes, Bernal, Argentina

[‡]CONICET, Argentina

Abstract—Generally, a grid-connected wave energy conversion system consists of various standard stages, such as wave absorption, power take-off, and power conditioning. Each stage has a specific control objective, which may not align with the control objectives of other stages, affecting overall wave-to-grid economic performance. This study assesses a controlled grid-connected wave energy conversion system with an improved reactive hydrodynamic WEC controller, i.e. LiTe-Con+. In particular, the LiTe-Con+ adapts its constraint handling mechanism in a time-varying manner, providing improved power absorption and use of the dynamic range. Lyapunov-based nonlinear controllers are also designed for the power converters in the powertrain. The proposed system is then simulated in the MATLAB/SIMULINK environment in order to demonstrate the effectiveness of the proposed control scheme. The results show the superior performance of LiTe-Con+ compared to LiTe-Con and passive damping controllers.

Index Terms—LiTe-Con+, Wave-to-grid control, grid integration

I. INTRODUCTION

A vital step in achieving a low-carbon economy and addressing the global challenge of climate change is the implementation of renewable energy alternatives. The use of renewable energy sources has been recognised as a critical strategy for combating anthropogenic climate change. These energy sources are regarded as sustainable because they are naturally replenished and do not produce greenhouse gases. Among these renewable energy sources, wave energy provides an abundant potential for clean energy [1] and is a relatively unexploited renewable resource. Developers and researchers have designed several wave energy converter (WEC) concepts [2] in recent years to harness the wave energy resource. However, one of the main reasons that wave energy has yet to reach commercial maturity is the difficulty of harnessing the reciprocating wave resource. In this regard, WEC control technology is considered critical for the economic viability of wave energy.

In general, WEC control systems are designed to maximise energy absorption subject to physical constraints, such as

displacement, velocity and power take-off (PTO) force constraints. Numerous control strategies have been proposed for WECs [3], ranging from relatively *simple* WEC controllers [4] to optimisation-based WEC controllers [5]. Additionally, the constraints handling is a vital part of the WEC control system, which is essential for the safety of the device. However, the imposition of constraints may result in conservative energy absorption. Hence, efficient constraint handling becomes critical since it affects the overall energy absorption capability of the wave energy conversion system. In the wave energy literature involving grid integration of WECs, passive damping hydrodynamic control is the default choice to maximise energy absorption [6]–[19]. For example, in a recent study [19], a nonlinear hydrodynamic model is proposed for grid integration of a WEC. However, a passive hydrodynamic control is used for maximum power absorption. Passive damping controllers have a narrow-banded absorption capability, with a significantly lower power absorption performance than reactive controllers (see, e.g. [20]), and they do not provide an intrinsic, theoretically-based, constraint handling method. As a result, passive damping controllers do not accurately picture the problems associated with grid-connected wave energy systems. On the other hand, reactive hydrodynamic WEC controllers provide better power absorption capability, but they affect overall wave-to-grid (W2G) performance. In particular, the reactive (reverse) power requirements of the reactive hydrodynamic WEC controllers add an additional difficulty in implementing the W2G control scheme [20]. To the best of the authors' knowledge, only one study in the grid-connected WECs literature includes a reactive hydrodynamic control, i.e. LiTe-Con (Linear Time invariant Controller) in [20]. However, the LiTe-Con controller uses a static constraint handling mechanism, which results in conservative energy absorption. This paper presents an improved time-varying reactive hydrodynamic control, i.e. LiTe-Con+ [21], for a grid-connected wave energy conversion system. The proposed approach uses a time-varying methodology for motion constraint handling based on excitation force envelope estimation, which is inspired by the Hilbert-Huang transform (HHT) [22]. As a result, the LiTe-Con+ maintains the simplicity

This work is supported by MaREI, the Science Foundation Ireland (SFI) Research Centre for Energy, Climate and Marine under Grant 12/RC/2302_P2.

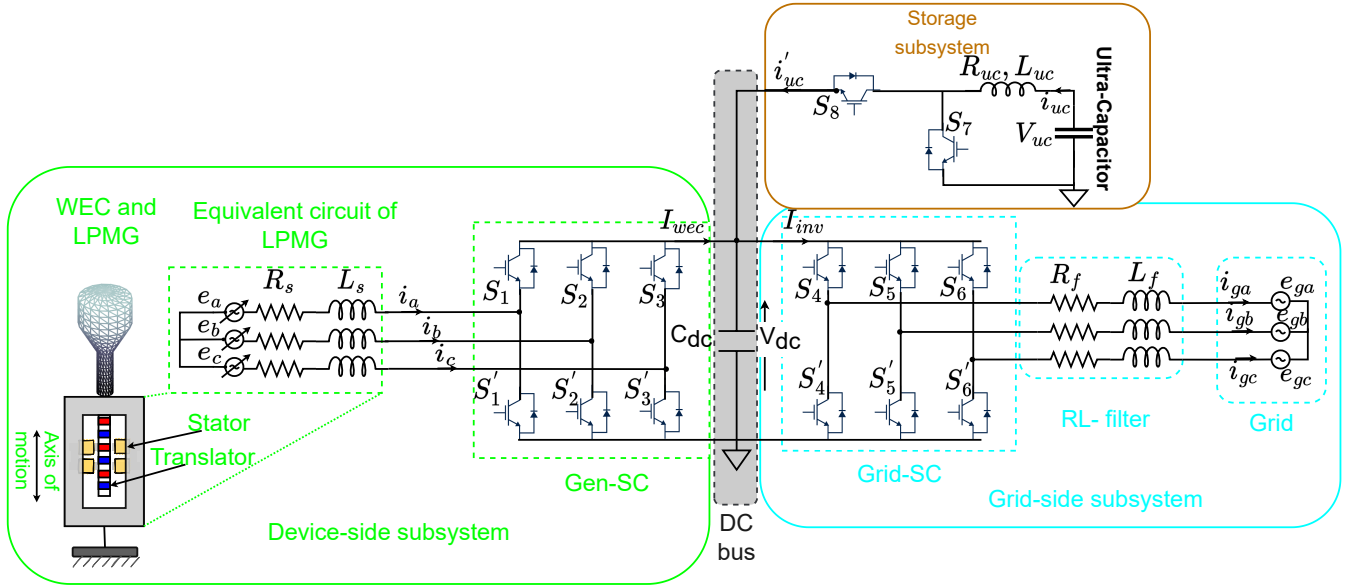


Fig. 1. Proposed grid-connected wave energy conversion system [20].

and efficiency of LiTe-Con, while providing a more effective time-varying constraint handling mechanism. In this paper, the LiTe-Con+ is implemented in a complete W2G coordinated control framework, showing the improved power absorption performance compared to the LiTe-Con, preserving the device within the physical constraints.

In this study, a direct-drive wave energy conversion system is considered. The W2G system consists of a point absorber WEC, constrained to move in the heave direction, a linear permanent magnet generator (LPMG), and back-to-back power converters with a DC-bus in-between, as shown in Fig. 1. An ultra-capacitor (UC) storage system is also a part of the powertrain.

The remainder of the paper is organised as follows. Section II details W2G modelling, including models for device-side subsystem, grid-side subsystem, and storage subsystem, while Section III describes W2G coordinated control scheme, with a focus on improved reactive hydrodynamic WEC control, i.e. LiTe-Con+. Results and discussion are detailed in Section IV, with Section V concludes this study.

II. W2G SYSTEM MODELLING

As shown in Fig 1, the W2G system includes a direct drive heaving point absorber WEC connected to the electric grid via back-to-back power converters, with UC-based short-term storage connected at the DC link. The models for each part of the powertrain are described in the following sections.

A. WEC modelling

This section describes a linear hydrodynamic WEC model based on the linear potential flow theory (LPT) [23]. Under the LPT assumptions, such as the fluid is irrotational, inviscid

and incompressible, the dynamics of the WEC, in the time-domain, can be written as

$$M\ddot{z}(t) = f_e(t) + f_r(t) + f_h(t) - f_{pto}(t), \quad (1)$$

where $f_e(t)$ is the uncontrollable excitation force acting on the WEC (external input), $f_r(t)$ is the radiation force and f_h is the hydrostatic stiffness (restoring) force. $f_{pto}(t)$ is the PTO force (control input) applied by the LPMG on the WEC. The mass of the oscillating system is represented by M , while the heave displacement is denoted by $z(t)$. The linearised hydrostatic stiffness force is given by¹:

$$f_h = -K_h z, \quad (2)$$

where $K_h > 0$ is the hydrostatic stiffness coefficient. The radiation force f_r , representing the fluid memory effects, is modelled through LPT, using Cummins' equation [24], as

$$f_r = -m_\infty \ddot{z} - k_r * \dot{z}, \quad (3)$$

where $m_\infty = \lim_{\omega \rightarrow +\infty} A(\omega)$ is the added mass at infinite frequency, with $A(\omega)$ representing the so-called radiation added mass, and k_r is the (causal) radiation impulse response function. The $*$ depicts the convolution operator. Finally, the complete equation of motion, from (1), is given by:

$$\mathcal{M}\ddot{z} + k_r * \dot{z} + K_h z = f_e - f_{pto}, \quad (4)$$

where $\mathcal{M} = M + m_\infty$. It is worth mentioning that the radiation convolution term $k_r * \dot{z}$ is computationally expensive and, therefore, it is generally approximated by a linear time invariant (LTI) state-space system [25]. In this regard, standard system identification toolboxes are developed in wave energy field as,

¹From now on, the dependence on t is dropped when clear from the context.

for example, the FOAMM toolbox [26], which computes an LTI approximation of the convolution term $k_r * \dot{z}$ as follows:

$$\begin{aligned} \dot{Y}_r &= A_r Y_r + B_r \dot{z}, \\ f_{rc} &= C_r Y_r \approx k_r * \dot{z}, \end{aligned} \quad (5)$$

where A_r , B_r and C_r are the state, input and output matrices of the LTI state-space approximation. Alternatively, the dynamics of the WEC can be characterised by a frequency-domain mapping $G(j\omega)$ as:

$$G(j\omega) = \frac{j\omega}{K_h - \omega^2 \mathcal{M} + j\omega K_r(j\omega)}, \quad (6)$$

with

$$V(j\omega) = G(j\omega)[F_e(j\omega) - F_{pto}(j\omega)]. \quad (7)$$

B. Electrical system modelling

In the direct drive powertrain considered here, the electrical system comprises an LPMG, a generator-side converter (Gen-SC), a grid-side converter (Grid-SC), and a DC/DC buck-boost converter for UC storage, as shown in Fig. 1. The models for each component are detailed in the following sections.

1) *LPMG and Gen-SC modelling*: In the d - q synchronous frame of reference, the LPMG dynamics is given in [27], as:

$$\frac{di_{ds}}{dt} = -\frac{R_s}{L_s} i_{ds} + \omega_e i_{qs} - \frac{1}{L_s} v_{ds}, \quad (8)$$

$$\frac{di_{qs}}{dt} = -\omega_e i_{ds} - \frac{R_s}{L_s} i_{qs} - \frac{\omega_e}{L_s} \psi_{PM} - \frac{1}{L_s} v_{qs}, \quad (9)$$

with,

$$f_{pto} = -1.5 \frac{\pi}{\tau} \psi_{PM} i_{qs}, \quad (10)$$

where $v_{ds,qs}$ and $i_{ds,qs}$ are the d - and q -axis stator voltages and currents respectively, ψ_{PM} is the permanent magnet flux linkage, L_s and R_s are the stator inductance and resistance respectively. ω_e represents the electrical angular velocity, computed as:

$$\omega_e = \frac{\pi}{\tau} \dot{z}, \quad (11)$$

where τ is the pole pitch of the LPMG. The voltages on stator $v_{ds,qs}$ are the input voltages for the Gen-SC and can be controlled independently. Therefore, the voltages are specified as corresponding converter control actions [28], [29], as follows:

$$v_{ds} = v_{dc} u_{ds}, \quad v_{qs} = v_{dc} u_{qs}, \quad (12)$$

where u_{ds} and u_{qs} are the d - q transformation of S_i , $\forall i = 1, 2, 3$, (see Fig. 1), defined as:

$$S_i = \begin{cases} 1 & \text{if } S_i \text{ is ON and } S'_i \text{ is OFF} \\ 0 & \text{if } S_i \text{ is OFF and } S'_i \text{ is ON} \end{cases} \quad (13)$$

Substituting the values of v_{ds} and v_{qs} from (12) into (8) and (9) results in the unified model for the LPMG and Gen-SC as follows:

$$\frac{di_{ds}}{dt} = -\frac{R_s}{L_s} i_{ds} + \omega_e i_{qs} - \frac{1}{L_s} v_{dc} u_{ds}, \quad (14)$$

$$\frac{di_{qs}}{dt} = -\omega_e i_{ds} - \frac{R_s}{L_s} i_{qs} - \frac{\omega_e}{L_s} \psi_{PM} - \frac{1}{L_s} v_{dc} u_{qs}. \quad (15)$$

2) *Grid-SC modelling*: The dynamic model for Grid-SC can be obtained [28], using the d - q transformation, as follows:

$$\frac{di_{dg}}{dt} = -\frac{V_{dg}}{L_f} + \omega_o i_{qg} - \frac{R_f}{L_f} i_{dg} + \frac{v_{dc}}{L_f} u_{dg}, \quad (16)$$

$$\frac{di_{qg}}{dt} = -\frac{V_{qg}}{L_f} - \omega_o i_{dg} - \frac{R_f}{L_f} i_{qg} + \frac{v_{dc}}{L_f} u_{qg}, \quad (17)$$

where, $i_{dg,qg}$ and $V_{dg,qg}$ denote the grid currents and voltages, respectively. R_f and L_f are the filter resistance and inductance, respectively, and $u_{dg,qg}$ are the d - q components of S_j , $\forall j = 4, 5, 6$ (see Fig. 1), defined as:

$$S_j = \begin{cases} 1 & \text{if } S_j \text{ is ON and } S'_j \text{ is OFF} \\ 0 & \text{if } S_j \text{ is OFF and } S'_j \text{ is ON} \end{cases} \quad (18)$$

3) *Buck-boost converter model for UC storage*: Buck-boost converters can operate in both boost and buck modes depending on power flow direction. During UC discharge mode, the converter works in boost mode (S_7 ON, S_8 OFF), thereby allowing the UC to supply power to the DC link. Conversely, during charge mode, the converter operates in buck mode (S_7 OFF, S_8 ON), charging the UC from the DC bus. The dynamics of the buck-boost converter can be derived as:

$$\frac{di_{uc}}{dt} = \frac{V_{uc}}{L_{uc}} - \frac{R_{uc}}{L_{uc}} i_{uc} - \frac{v_{dc}}{L_{uc}} u_{78}, \quad (19)$$

$$i'_{uc} = u_{78} i_{uc}, \quad (20)$$

where V_{uc} , L_{uc} , and R_{uc} denote the UC voltage, inductance and equivalent series resistance, respectively. The UC input and output currents are denoted by i_{uc} and i'_{uc} , respectively. For simplicity, u_{78} is parameterised as:

$$u_{78} = N(1 - u_7) + (1 - N)u_8, \quad (21)$$

where u_7 and u_8 representing the control signals for the switches S_7 and S_8 , respectively. Moreover, N is defined as:

$$N = \begin{cases} 1 & \text{if } S_7 \text{ is ON and } S_8 \text{ is OFF (Boost mode)} \\ 0 & \text{if } S_7 \text{ is OFF and } S_8 \text{ is ON (Buck mode)} \end{cases}$$

4) *Combined electrical system model*: The mathematical models presented in Sections II-B1, II-B2 and II-B3, for the LPMG, Gen-SC, Grid-SC, and buck-boost converter, respec-

tively, are combined to get a complete electrical system model, using the state-space averaging method², as follows:

$$\frac{dx_1}{dt} = -\frac{R_s}{L_s}x_1 + \omega_e x_2 - \frac{x_6}{L_s}\mu_{ds}, \quad (22)$$

$$\frac{dx_2}{dt} = -\omega_e x_1 - \frac{R_s}{L_s}x_2 - \frac{\omega_e}{L_s}\psi_{PM} - \frac{x_6}{L_s}\mu_{qs}, \quad (23)$$

$$\frac{dx_3}{dt} = -\frac{V_{dg}}{L_f} - \frac{R_f}{L_f}x_3 + \omega_o x_4 + \frac{x_6}{L_f}\mu_{dg}, \quad (24)$$

$$\frac{dx_4}{dt} = -\frac{V_{qg}}{L_f} - \omega_o x_3 - \frac{R_f}{L_f}x_4 + \frac{x_6}{L_f}\mu_{qg}, \quad (25)$$

$$\frac{dx_5}{dt} = \frac{V_{uc}}{L_{uc}} - \frac{R_{uc}}{L_{uc}}x_5 - \frac{x_6}{L_{uc}}\mu_{78}, \quad (26)$$

$$\frac{dx_6}{dt} = \frac{1}{C_{dc}}[(\mu_{ds}x_1 + \mu_{qs}x_2) + \mu_{78}x_5 - i_{inv}], \quad (27)$$

with $x_1 = \langle i_{ds} \rangle$, $x_2 = \langle i_{qs} \rangle$, $x_3 = \langle i_{dg} \rangle$, $x_4 = \langle i_{qg} \rangle$, $x_5 = \langle i_{uc} \rangle$ and $x_6 = \langle V_{dc} \rangle$, where the operator $\langle \cdot \rangle$ represents the average value over a switching period, and μ_{ds} , μ_{qs} , μ_{dg} , μ_{qg} , and μ_{78} are the control signals for the Gen-SC, Grid-SC and buck-boost converter, respectively.

III. W2G COORDINATED CONTROL

A. LiTe-Con+ (hydrodynamic control)

The LiTe-Con+ represents an immediate extension to the LiTe-Con energy maximising control strategy for WEC systems [21]. While the LiTe-Con has shown effectiveness, considering a broad set of different conditions and operating scenarios, even in experimental environments, its constraint handling mechanism, based on a static gain, can limit the overall control performance. In other words, the LiTe-Con can produce conservative results, mainly in operating scenarios where displacement limits are frequently reached. To address this limitation, the LiTe-Con+ adopts a dynamical, i.e. a time-variant, constraint handling strategy, based on an online estimation of the envelope of the excitation force. It is worth highlighting that, from the WEC system point of view, the excitation force is an exogenous factor and, under linear operating conditions, does not depend on the instantaneous dynamics of the system. This crucial aspect decouples the constraint handling action from the system motion, which significantly simplifies the application of this control strategy from, for example, the stability perspective. Thus, by estimating the excitation force envelope in real-time, the LiTe-Con+ can provide a more effective control action, increasing the amount of absorbed energy.

The implementation of the LiTe-Con+ can be divided into three distinct stages. Firstly, based on the impedance-matching theory, an optimal control condition is formulated and approximated using a LTI structure. The second stage computes an online envelope estimation of the excitation force, which can be obtained through standard methodologies. Specifically, the envelope estimation methodology proposed in [21], and considered for this study, is inspired by the Hilbert-Huang

²The interested readers are referred to [30] for a detailed discussion on averaging methods for power conversion circuits.

transform, which is a widely used technique in signal processing [22]. Finally, in the third stage, a dynamical mapping is defined to link the obtained instantaneous envelope estimation and the resulting constraint handling gain, which is a time-varying gain, in contrast with the static one in the LiTe-Con. Each of the three described stages are detailed in Fig. 2, where each one is indicated by 1, 2, and 3, within circular containers, while the LTI optimal control structure, denoted with the block labelled as \tilde{H}_{ff} , the dynamical mapping, labelled as \mathcal{K} , and the time-varying gain, $k(t)$ are shown. Each of the aforementioned stages are described in detail below.

1) *Optimal control condition - LiTe-Con*: The impedance-matching theory [23], based on linear assumptions, enables us to determine an optimal condition that can be described in relation to a optimal velocity profile, $V^{opt}(\omega)$, as

$$V^{opt}(\omega) = \frac{1}{Z_i(\omega) + Z_i^*(\omega)} F_e(\omega) = \frac{1}{2B_r(\omega)} F_e(\omega), \quad (28)$$

where $Z_i^*(\omega)$ represents the complex conjugate of $Z_i(\omega)$. Eq. (28) defines a purely real mapping, guaranteeing a zero-phase-locking condition between the device velocity and $f_e(t)$. However, standard results for impedance-matching-based control cannot be straightforwardly implementable in practice and require practical consideration for implementation [4].

With the aim of finding an implementable structure for WEC control considering such an impedance-matching condition, the frequency-domain description of the system $G_0(s)$ can be expressed as³:

$$G_0(s) \Big|_{s=j\omega} = \Re(G) + j\Im(G). \quad (29)$$

Therefore, it is feasible to present an alternative expression for the optimal relationship between $F_e(\omega)$ and $V^{opt}(\omega)$, as shown in (28), such that:

$$\frac{V^{opt}(\omega)}{F_e(\omega)} = T_{f_e \rightarrow v}^{opt}(\omega) = \frac{\Re(G)^2 + \Im(G)^2}{2\Re(G)}. \quad (30)$$

The optimal control condition, expressed in (30), can be accomplished through a feed-forward (FF) control configuration, indicated in the following expression:

$$H_{ff}(\omega) = \frac{\Re(G) + j\Im(G)}{2\Re(G)}, \quad (31)$$

such that:

$$T_{f_e \rightarrow v}^{opt}(\omega) = (1 - H_{ff}(\omega)) G_0(j\omega). \quad (32)$$

Frequency-domain system identification techniques [31] can be employed to estimate $H_{ff}(j\omega)$, which can be approximated using a stable and feasible LTI dynamic system denoted as $\tilde{H}_{ff}(s)$, i.e.:

$$\tilde{H}_{ff}(s) \Big|_{s=j\omega} \approx H_{ff}(\omega). \quad (33)$$

³For the sake of simplicity of notation, let $\Re(G) = \Re\{G(j\omega)\}$ and $\Im(G) = \Im\{G(j\omega)\}$ denote the *real-part* and *imaginary-part* operators, respectively.

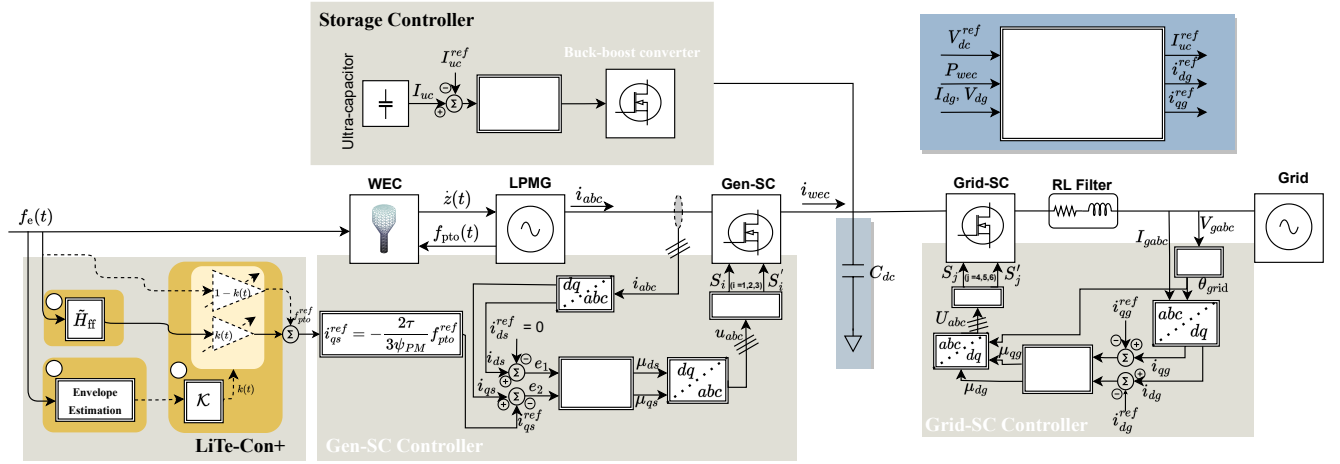


Fig. 2. W2G control block diagram.

The LiTe-Con combines the approach outlined in (32) with a static constraint management mechanism that involves a fixed constant value of k within the range of $[0, 1]$. As a result, the reference for the control force (PTO) $f_{pto}^{ref}(t)$ is:

$$f_{pto}^{ref}(t) = \left[k\tilde{H}_{ff}(s) + (1 - k) \right] \hat{f}_e(t), \quad (34)$$

where $\hat{f}_e(t)$ is an estimate of $f_e(t)$. Eq. (34) implies that when $k = 1$, the controller coincides with the optimal expression presented in equation (30), whereas when $k = 0$, the force-to-velocity mapping output is set to zero, thereby halting the device motion (assuming an ideal estimation of $f_e(t)$). For a detailed discussion on the design and tuning of the LiTe-Con methodology, specifically its constraint handling mechanism, the reader is referred to [32].

Note that the primary difference between the LiTe-Con (see Eq. (34)) and LiTe-Con+ is attributed to the nature of gain k . Specifically, in the LiTe-Con+, as shown in Fig. 2, the gain for constraint handling is a time-varying one, which is defined time-by-time, as explained in the following.

2) *Envelope estimation*: The adaptation of constraint handling gain in the LiTe-Con+ is based on an online estimation of the envelope of the excitation force, which is generally considered to be a quasi-periodic single-frequency non-stationary process within a wave energy framework [33]:

$$f_e(t) \approx E(t) \cos \left(\int \omega_e(t) dt \right), \quad (35)$$

where $E(t)$ denotes the instantaneous amplitude of $f_e(t)$. This study employs the HHT-inspired methodology presented in [21] to estimate $E(t)$, denoted in this study as $\hat{E}(t)$. In general, the envelope estimation approach involves interpolating the set of local maxima of $|f_e(t)|$, P_k , within a time window that spans both past and, if available, future values of $f_e(t)$, for which a forecasting strategy can be used. Fig. 3 illustrates the typical steps involved in estimating the envelope. The key components of the algorithm include identifying the set

of local maxima P_k within the total time window, obtaining the absolute value of $f_e(t)$, and determining the current time (t_0) and the envelope estimation ($\hat{E}(t_0)$). In addition, the

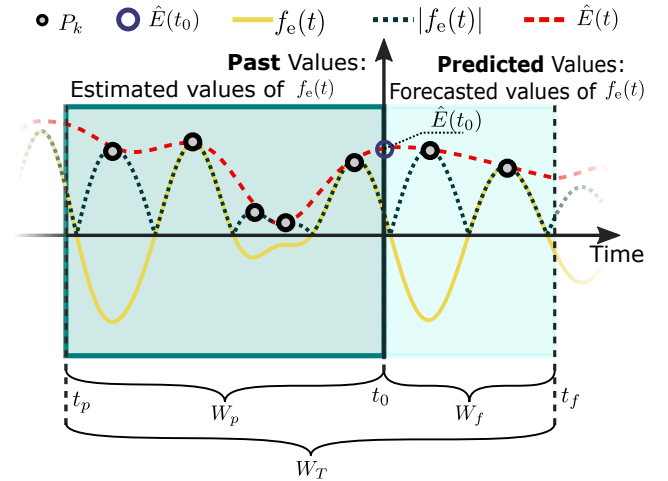


Fig. 3. Envelope estimation algorithm (adapted from [21]).

time-windows of past and predicted values have lengths W_p and W_f , respectively, i.e. $W_T = W_p + W_f$, are shown in Fig. 3. Lastly, the estimation of $\hat{E}(t)$ can be achieved by interpolating the local maxima set P_k through standard interpolation techniques, such as cubic spline interpolation, as discussed in [21].

3) *Dynamical mapping and constraint gain*: To achieve the desired time-varying modulation of the gain k , obtaining a time-varying version of (34), a mapping $\mathcal{K} : \mathbb{R}^+ \mapsto [k_{min}, k_{max}]$ is needed. This mapping transforms the estimated envelope into the resulting modulation of k , and must be strictly decreasing by definition. To define this mapping, at least three tuning parameters are necessary: an estimate of the expected maximum value of the envelope E_{max} , and the minimum and maximum interval limits for the modulation of

$k(t)$, denoted as k_{min} and k_{max} , respectively. A set of curves given by the exponential family:

$$\mathcal{K} : k(t) = \begin{cases} \kappa_1 e^{\kappa_2 E(t)} + \kappa_3 & \text{if } 0 \leq \hat{E}(t) \leq E_{max} \\ k_{min} & \text{if } \hat{E}(t) > E_{max} \end{cases} \quad (36)$$

is shown in Fig. 4, using a solid line for the linear case, while κ_1 , κ_2 , and $\kappa_3 \in \mathbb{R}$, in (36) can be easily fitted using basic curve fitting algorithms, with E_{max} , k_{min} , and k_{max} .

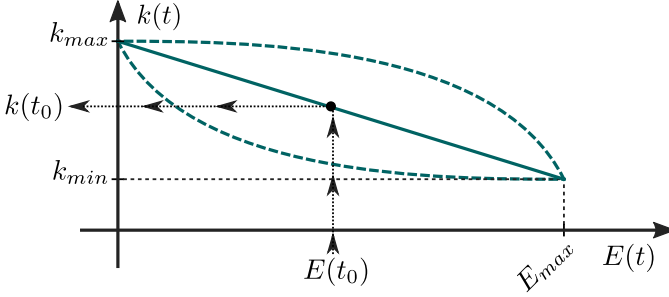


Fig. 4. Various possibilities for mapping \mathcal{K} .

Now, the (34) can be updated to show the time-varying constraint handling gain $k(t)$ as follows:

$$f_{pto}^{ref}(t) = \left[k(t) \tilde{H}_{ff}(s) + (1 - k(t)) \right] f_c(t). \quad (37)$$

B. Electrical system control

Control of power converters, including the Gen-SC, Grid-SC, and Buck-boost converter for the storage system in the powertrain, falls under the purview of electrical system control. Nonlinear controllers based on Lyapunov methods, as described in [20], have been developed for each converter in the powertrain. The details of each converter control are given in the following.

1) *Gen-SC control*: Gen-SC control aims to achieve two primary objectives: maximising power absorption from waves and minimising Copper loss (Cu-loss). Maximum power absorption is performed by tracking the reference PTO (LPMG) force, given in (37), provided by the LiTe-Con+. To achieve this, the PTO force reference $f_{pto}^{ref}(t)$ is utilised to generate the current reference i_{qs}^{ref} , by using (10), which is then used for Gen-SC control.

$$i_{qs}^{ref} = -\frac{2\tau}{3\psi_{PM}} f_{pto}^{ref}. \quad (38)$$

Additionally, i_{ds}^{ref} is set to zero for Cu-loss minimisation. Finally, the Lyapunov-based control laws, aiming to track LPMG stator d - and q -axis current references are given below⁴ [20]:

$$\mu_{ds} = \frac{1}{x_6} [-R_s x_1 + \omega_e L_s x_2 + c_1 e_1 L_s - L_s i_{ds}^{ref}], \quad (39)$$

$$\mu_{qs} = \frac{1}{x_6} [-\omega_e L_s x_1 - R_s x_2 - \omega_e \psi_{PM} + c_2 e_2 L_s - L_s i_{qs}^{ref}], \quad (40)$$

⁴For a comprehensive description on the design and stability analysis of Lyapunov-based controllers, the readers are referred to [20].

where $c_1 > 0$ and $c_2 > 0$, are the controller design parameters. The LiTeCon+ and Gen-SC controllers make the complete device-side control system schematically shown in Fig. 2.

2) *Grid-SC control*: The objectives of Grid-SC control are centred around injecting maximum active power into the grid while maintaining zero reactive electrical power injection. A synchronous reference frame-phase locked loop (SRF-PLL) synchronises inverter and grid voltages. Maximum active power is injected to the grid by tracking d -axis current reference i_{dg}^{ref} , while the q -axis current reference i_{qg}^{ref} is set to zero for zero reactive electrical power injection under normal grid operation. In the event of voltage sags or grid faults, the q -axis current reference i_{qg}^{ref} is updated to provide reactive electrical power and maintain grid stability. The d - and q -axis current references are generated using an energy management system (EMS) detailed in Section III-C. Lyapunov-based control laws designed to track inverter d - and q -axis current references are given below:

$$\mu_{dg} = \frac{1}{x_6} [R_f x_3 + \omega_o L_f x_4 + V_{dg} - c_3 e_3 L_f + L_f i_{dg}^{ref}], \quad (41)$$

$$\mu_{qg} = \frac{1}{x_6} [\omega_o L_f x_3 + R_f x_4 + V_{qg} - c_4 e_4 L_f + L_f i_{qg}^{ref}], \quad (42)$$

where $c_3 > 0$ and $c_4 > 0$, are additional design parameters.

3) *Buck-boost converter control for storage subsystem*: A short-term UC-based storage system is employed to carry out three tasks, namely: (1) support for reactive hydrodynamic control, (2) improvement of power quality, and (3) grid support during grid faults. In particular, reactive hydrodynamic control support is accomplished by supplying reactive⁵ (reverse) power to the LPMG, when required [20]. Power quality is improved by DC-bus voltage regulation. Finally, the grid faults are supported by the UC storage by providing electrical reactive power during grid faults [34]. Each of these task is achieved by controlling DC/DC buck-boost converter by tracking a UC current reference I_{uc}^{ref} , provided by the EMS (supervisory control) presented in Section III-C. Finally, a Lyapunov-based nonlinear controller is designed to track I_{uc}^{ref} as given below:

$$\mu_{78} = \frac{1}{x_6} [V_{uc} - R_{uc} x_5 + c_5 e_5 L_{uc} - e_6 L_{uc} - L_{uc} I_{uc}^{ref}] \quad (43)$$

where $c_5 > 0$ is a further design parameter.

C. Energy management system

The energy management system (EMS) serves as a high-level supervisory control mechanism that generates reference signals for the low-level power converter controllers. Specifically, the EMS is tasked with ensuring W2G controlled operation is maintained at all times by managing the buck-boost converter for the storage system and Grid-SC. Fig. 5

⁵The interested reader is referred to [20] for a complete description of the differences between reactive power in hydrodynamic control sense and reactive power in electrical networks.

illustrates the overview of EMS, considered here, under both normal and fault conditions. Depending upon the operation

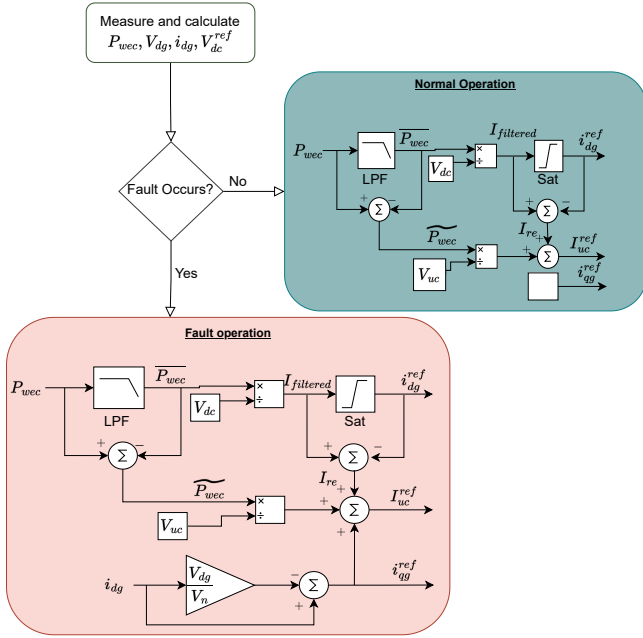


Fig. 5. Energy management system overview [34].

mode (normal or grid-fault mode), EMS provides reference signals to the buck-boost storage converter and Grid-SC accordingly. Under normal operation, the EMS ensures that the UC storage system performs two tasks: regulating the DC bus voltage and providing support for reactive hydrodynamic control (LiTe-Con+) by generating a UC current reference I_{uc}^{ref} . In addition, EMS also provides reference signals, i.e. i_{dg}^{ref} and i_{qg}^{ref} , for Grid-SC controllers. In summary, the WEC output power (P_{wec}) is split into high- and low-frequency components by utilising a low-pass filter, as shown in Fig. 5. The high-frequency component (\widetilde{P}_{wec}) is used to generate UC storage current reference I_{uc}^{ref} , which absorbs high-frequency fluctuations in the output power and regulates DC-bus voltage. Moreover, the saturation block in Fig. 5 ensures that the UC storage system provides the reverse (reactive) power required for LiTe-Con+. The low-frequency component (\overline{P}_{wec}), on the other hand, is utilised to generate the i_{dg}^{ref} current reference for maximum active power injection to the grid via the Grid-SC. For unity power factor control, i_{qg}^{ref} is set to zero. In the event of voltage sags or grid faults, the EMS system ensures that the UC storage system provides support by supplying a i_{qg} current proportional to the voltage sag. Consequently, i_{qg}^{ref} is non-zero during such conditions, as depicted in Fig. 5.

IV. RESULTS AND DISCUSSION

The proposed control scheme for the grid-connected wave energy conversion system is evaluated through simulations in the MATLAB/SIMULINK environment. In this regard, an irregular wave model, based on a JONSWAP spectrum [35], is utilised to generate free-surface elevation, which is then used

to generate excitation force f_e . The sea-states considered have a fixed significant wave height of $H_s = 2$ [m], with the peak wave period T_p in the range $T_p \in [5, 12]$ [s] and a peak shape parameter $\gamma = 3.3$. To obtain statistically consistent results, 20 realisations of each sea state are considered, with the length of each realisation being 200 times the peak wave period T_p .

Fig. 6 compares the proposed LiTe-Con+ controller with the LiTe-Con and passive damping controllers. In particular, Fig. 6(a) provides results for absorbed power, and it is clear that the LiTe-Con+ consistently performs better than LiTe-Con for the same position constraints, i.e. $[-1.5, 1.5]$ [m], due to better utilisation of operational range. Consequently, the converted electrical power, presented in Fig. 6(b), is also greater for LiTe-Con+ than LiTe-Con. However, at longer periods, i.e. $T_p > 10$ [s], the difference between LiTe-Con+ and LiTe-Con is minimal due to the increased Cu-losses in the stator of LPMG. Additionally, both LiTe-Con+ and LiTe-Con outperforms passive damping controller due to broadband nature of these reactive controllers. In Fig. 6(c), the PTAP ratios for all controllers are presented, indicating that the passive damping controller consistently has lower PTAP ratios (around ten) compared to both LiTe-Con+ and LiTe-Con controllers. This is due to the fact that passive damping controllers have narrow banded power absorption capability and require lower peak PTO forces. On the other hand, both LiTe-Con+ and LiTe-Con have consistently higher PTAP ratios than passive damping controller due to higher peak PTO force requirements, translating into high output power peaks. Interestingly, LiTe-Con+ has lower PTAP ratios as compared to LiTe-Con due to increased average absorbed power (see Fig. 6(a)) with LiTe-Con+. Hence, LiTe-Con+ improves power absorption performance, which results in lower PTAP ratios than LiTe-Con. Fig. 6(d) depicts each controller's maximum PTO control force requirement for the range of wave periods considered here. As expected, both LiTe-Con+ and LiTe-Con have more peak PTO force requirements than the passive damping controller due to their broadband reactive nature. Moreover, LiTe-Con+ and LiTe-Con have similar peak PTO force requirements for most sea-states, as illustrated in Fig. 6(d), which shows the better use of operational range due to an improved time-varying constraint handling mechanism for LiTe-Con+.

The improved performance of the LiTe-Con+ is attributed to the controller's ability to optimise better usage of the operational range, which is further demonstrated in Fig. 7. In particular, a histogram is presented in Fig. 7 to illustrate the operation range of both LiTe-Con+ and LiTe-Con, with 500 bins covering the range of $[-1.5, 1.5]$ [m]. The histogram shows the frequency of occurrences of the device displacement in each bin for both controllers. This histogram highlights the superior performance of the LiTe-Con+ in terms of increased usage of the operational range, a considerable improvement compared to the LiTe-Con controller. Furthermore, this histogram also illustrates that the LiTe-Con+ takes advantage of the entire operational range, with an increased frequency of occurrences around constraint limits, i.e. -1.5 [m] and 1.5

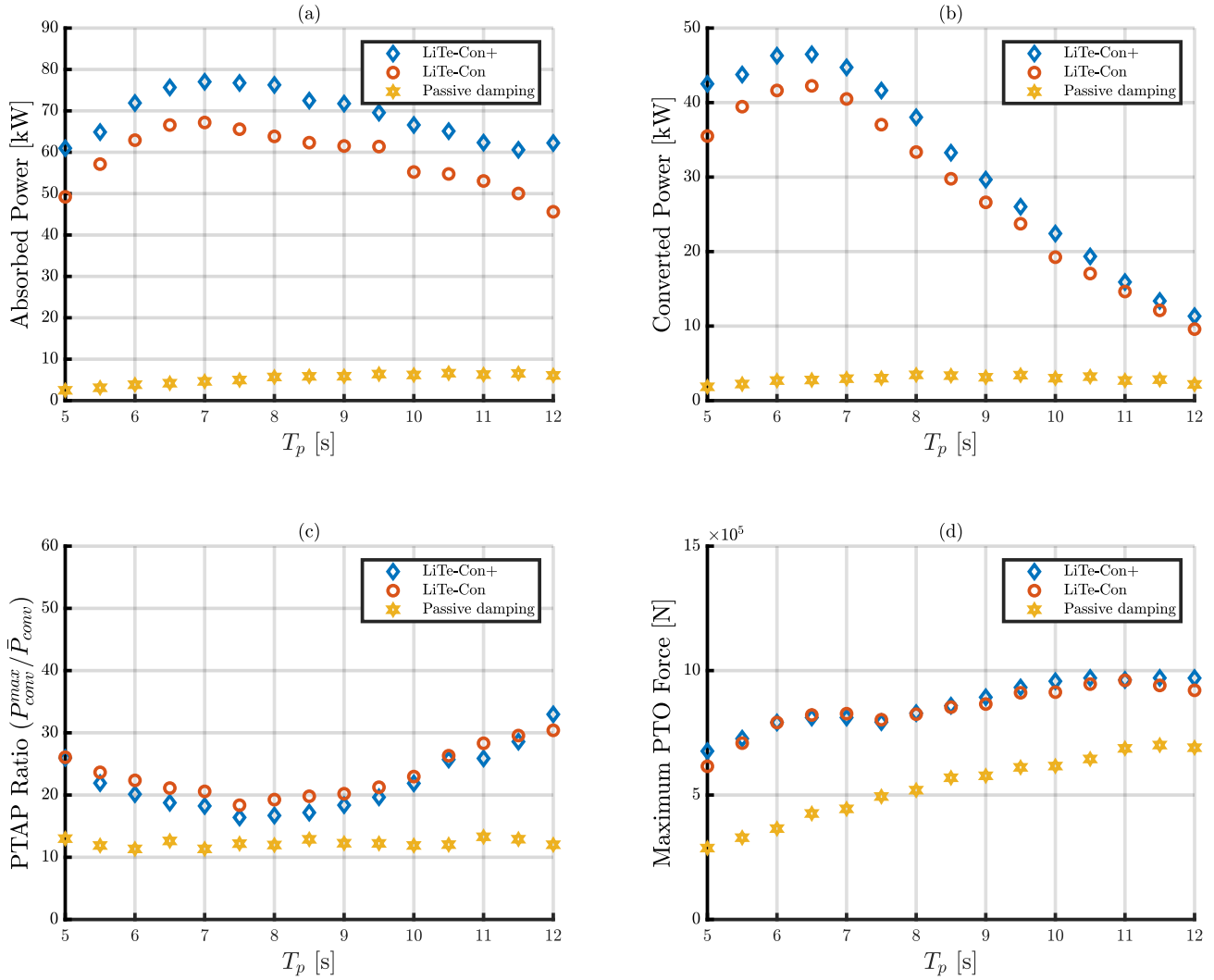


Fig. 6. Performance comparison of LiTe-Con+, LiTe-Con and passive damping control for the totality of sea-states considered. (a) Absorbed power [kW], (b) Converted power [kW], (c) Peak-to-average power ratio of the converted power, and (d) Maximum PTO (control) force [N]

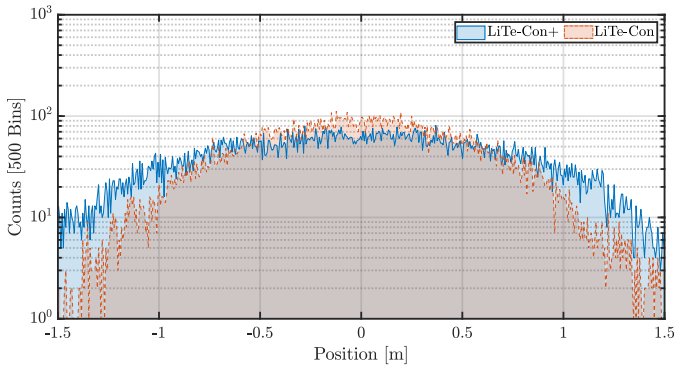


Fig. 7. Comparative analysis of dynamic range for LiTe-Con+ and LiTe-Con for a sea-state with $H_s = 2$ [m], $T_p = 8.5$ [s] and $\gamma = 3.3$. A histogram of operation range $[-1.5, 1.5]$ [m] with 500 bins is considered here.

[m]. Thus, the LiTe-Con+ controller employs a time-varying constraint handling mechanism that allows it to react faster to changes in the excitation force and ensures that it stays within its operating limits while effectively utilising its operating range.

V. CONCLUSIONS

This study presents a time-varying reactive hydrodynamic control (LiTe-Con+) as part of a W2G coordinated control strategy for a direct-drive wave energy conversion system. The LiTe-Con+ reactive hydrodynamic control utilises a time-varying constraint handling mechanism based on excitation force envelope estimation. The time-varying constraint handling in the LiTe-Con+ results in an overall better performance than LiTe-Con and passive damping control in terms of absorbed power by using the operational range effectively and preserving the device within the physical constraints. As a

result, PTAP ratios are lower for LiTe-Con+ than LiTe-Con, which are desirable for reducing PTO costs.

ACKNOWLEDGMENT

Thanks are due to CarrieAnne Barry of the Centre for Ocean Energy Research (COER) at Maynooth University for providing language help and proofreading the article. This work is supported by MaREI, the Science Foundation Ireland (SFI) Research Centre for Energy, Climate and Marine under Grant 12/RC/2302_P2.

REFERENCES

- [1] B. Reguero, I. Losada, and F. Méndez, "A global wave power resource and its seasonal, interannual and long-term variability," *Appl Energy*, vol. 148, pp. 366–380, 2015.
- [2] B. Guo and J. V. Ringwood, "A review of wave energy technology from a research and commercial perspective," *IET Renew. Power Gener.*, vol. 15, no. 14, pp. 3065–3090, 2021.
- [3] J. V. Ringwood, G. Bacelli, and F. Fusco, "Energy-maximizing control of wave-energy converters: The development of control system technology to optimize their operation," *IEEE Control Syst. Mag.*, vol. 34, no. 5, pp. 30–55, 2014.
- [4] D. García-Violini, N. Faedo, F. Jaramillo-Lopez, and J. V. Ringwood, "Simple controllers for wave energy devices compared," *J. Mar. Sci. Eng.*, vol. 8, no. 10, p. 793, 2020.
- [5] N. Faedo, S. Olaya, and J. V. Ringwood, "Optimal control, MPC and MPC-like algorithms for wave energy systems: An overview," *IFAC J. Syst. Control*, vol. 1, pp. 37–56, 2017.
- [6] H. A. Said and J. V. Ringwood, "Grid integration aspects of wave energy—Overview and perspectives," *IET Renew. Power Gener.*, vol. 15, no. 14, pp. 3045–3064, 2021.
- [7] F. Wu, X.-P. Zhang, P. Ju, and M. J. H. Sterling, "Modeling and control of AWS-based wave energy conversion system integrated into power grid," *IEEE Trans. Power Syst.*, vol. 23, no. 3, pp. 1196–1204, 2008.
- [8] F. Wu, X. P. Zhang, P. Ju, and M. J. H. Sterling, "Optimal control for AWS-based wave energy conversion system," *IEEE Trans. Power Syst.*, vol. 24, no. 4, pp. 1747–1755, 2009.
- [9] A. G. Santana, D. E. M. Andrade, and A. Jaén, "Control of hydrodynamic parameters of wave energy point absorbers using linear generators and VSC-based power converters connected to the grid," in *Int. J. Conf. Renew. Energies Power Qual. Spain*, 2010.
- [10] F. Wu, P. Ju, X.-P. Zhang, C. Qin, G.-J. Peng, H. Huang, and J. Fang, "Modeling, control strategy, and power conditioning for direct-drive wave energy conversion to operate with power grid," *Proc. IEEE*, vol. 101, no. 4, pp. 925–941, 2013.
- [11] M. I. Marei, M. Mokhtar, and A. A. El-Sattar, "MPPT strategy based on speed control for AWS-based wave energy conversion system," *Renew. Energy*, vol. 83, pp. 305–317, 2015.
- [12] S. Jafarishadeh, M. Farasat, and S. Mehraeen, "Grid-connected operation of direct-drive wave energy converter by using HVDC line and undersea storage system," in *2017 IEEE Energy Convers. Congr. Expo. IEEE*, 2017, pp. 5565–5571.
- [13] H. M. Hasanien, "Transient stability augmentation of a wave energy conversion system using a water cycle algorithm-based multiobjective optimal control strategy," *IEEE Trans. Ind. Informatics*, vol. 15, no. 6, pp. 3411–3419, 2018.
- [14] S. Rasool, M. R. Islam, K. M. Muttaqi, and D. Sutanto, "An advanced control strategy for a smooth integration of linear generator based wave energy conversion system with distribution power grids," in *2019 IEEE Ind. Appl. Soc. Annu. Meet. IEEE*, 2019, pp. 1–6.
- [15] K.-H. Lu, C.-M. Hong, Z. Han, and L. Yu, "New Intelligent Control Strategy Hybrid Grey-RCMAC Algorithm for Ocean Wave Power Generation Systems," *Energies*, vol. 13, no. 1, p. 241, 2020.
- [16] S. Rasool, M. R. Islam, K. M. Muttaqi, and D. Sutanto, "Coupled Modeling and Advanced Control for Smooth Operation of a Grid-Connected Linear Electric Generator Based Wave-to-Wire System," *IEEE Trans. Ind. Appl.*, vol. 56, no. 5, pp. 5575–5584, 2020.
- [17] A. Parwal, M. Fregelius, J. Leijon, M. Chatzigiannakou, O. Svensson, E. Strömstedt, I. Temiz, J. G. de Oliveira, C. Boström, and M. Leijon, "Grid integration and a power quality assessment of a wave-energy park," *IET Smart Grid*, vol. 2, no. 4, pp. 625–634, 2019.
- [18] A. Parwal, M. Fregelius, P. Almeida, O. Svensson, I. Temiz, J. G. Oliveira, C. Boström, and M. Leijon, "A Comparative Analysis of Linear and Nonlinear Control of Wave Energy Converter for a Force Control Application," *Int. Mar. Energy J.*, vol. 2, no. 1 (Nov), pp. 39–50, 2019.
- [19] A. Mahdy, H. M. Hasanien, W. H. A. Hameed, R. A. Turkey, S. H. A. Aleem, and E. A. Ebrahim, "Nonlinear modeling and real-time simulation of a grid-connected aws wave energy conversion system," *IEEE Trans. Sustain. Energ.*, vol. 13, no. 3, pp. 1744–1755, 2022.
- [20] H. A. Said, D. García-Violini, and J. V. Ringwood, "Wave-to-grid (W2G) control of a wave energy converter," *Energy Convers. Manage. : X*, vol. 14, p. 100190, 2022.
- [21] D. García-Violini, Y. Peña-Sanchez, N. Faedo, F. Ferri, and J. V. Ringwood, "A broadband time-varying energy maximising control for wave energy systems (LiTe-Con+): Framework and experimental assessment," *IEEE Trans. Sust. Energ.*, 2023.
- [22] N. E. Huang, Z. Shen, S. R. Long, M. C. Wu, H. H. Shih, Q. Zheng, N.-C. Yen, C. C. Tung, and H. H. Liu, "The empirical mode decomposition and the Hilbert spectrum for nonlinear and non-stationary time series analysis," *Proceedings of the Royal Society of London. Series A: mathematical, physical and engineering sciences*, vol. 454, no. 1971, pp. 903–995, 1998.
- [23] J. Falnes and A. Kurniawan, *Ocean waves and oscillating systems: linear interactions including wave-energy extraction*. Cambridge University Press, 2020, vol. 8.
- [24] W. Cummins, "The impulse response function and ship motions. DTIC Document," in *Proceeding Symp. Ship Theory Inst. für Schiffbau der Univ. Hamburg.*, 1962, pp. 25–27.
- [25] N. Faedo, Y. Peña-Sanchez, and J. V. Ringwood, "Finite-order hydrodynamic model determination for wave energy applications using moment-matching," *Ocean Eng.*, vol. 163, pp. 251–263, 2018.
- [26] Y. Peña-Sanchez, N. Faedo, M. Penalba, G. Giorgi, A. Mérigaud, C. Windt, D. García Violini, L. Wang, and J. V. Ringwood, "Finite-Order hydrodynamic Approximation by Moment-Matching (FOAMM) toolbox for wave energy applications," in *13th Eur. Wave Tidal Energy Conf. EWTEC, Naples, Italy*, 2019, pp. 1448–1:1448–9.
- [27] R. Krishna, O. Svensson, M. Rahm, S. K. Kottayil, R. Waters, and M. Leijon, "Analysis of linear wave power generator model with real sea experimental results," *IET Renew. Power Gener.*, vol. 7, no. 5, pp. 574–581, 2013.
- [28] A. El Magri, F. Giri, G. Besancon, A. El Fadili, L. Dugard, and F. Z. Chaoui, "Sensorless adaptive output feedback control of wind energy systems with PMS generators," *Control Eng. Pract.*, vol. 21, no. 4, pp. 530–543, 2013.
- [29] H. A. Said and J. V. Ringwood, "Intelligent control of a DC microgrid consisting of Wave Energy Converter (WEC) and Hybrid Energy Storage System (HESS)," in *14th Eur. Wave Tidal Energy Conf. EWTEC, Plymouth.*, 2021, pp. 1884–1:1884–9.
- [30] S. R. Sanders, J. M. Noworolski, X. Z. Liu, and G. C. Verghese, "Generalized averaging method for power conversion circuits," *IEEE Trans. Power Electron.*, vol. 6, no. 2, pp. 251–259, 1991.
- [31] L. Ljung, *System identification*. Springer, 1998.
- [32] D. García-Violini, Y. Peña-Sanchez, N. Faedo, and J. V. Ringwood, "An energy-maximising linear time invariant controller (LiTe-Con) for wave energy devices," *IEEE Trans. Sust. Energ.*, vol. 11, no. 4, pp. 2713–2721, 2020.
- [33] F. Fusco and J. V. Ringwood, "A simple and effective real-time controller for wave energy converters," *IEEE Trans. Sust. Energ.*, vol. 4, no. 1, pp. 21–30, 2013.
- [34] H. Said and J. Ringwood, "Low voltage ride-through capability enhancement of a grid-connected wave energy conversion system," in *Trends in Renew. Energ. Offshore, RENEW 2022, Lisbon*. CRC Press, 2022, pp. 267–275.
- [35] K. Hasselmann, T. P. Barnett, E. Bouws, H. Carlson, D. E. Cartwright, K. Enke, J. Ewing, A. Gienapp, D. Hasselmann, P. Kruseman *et al.*, "Measurements of wind-wave growth and swell decay during the joint north sea wave project (JONSWAP)." *Ergaenzungsheft zur Deutschen Hydrographischen Zeitschrift, Reihe A*, 1973.